Oxidation state and magnetic properties of $Pb_2Sr_2Tb_{1-x}Y_xCu_3O_8$

U. Staub, L. Soderholm, S. Skanthakumar, and Mark R. Antonio
Chemistry Division, Argonne National Laboratory, Argonne, Illinois 60439-4831
(Received 20 March 1995)

L_3-edge x-ray absorption, inelastic neutron scattering (INS), and magnetic susceptibility experiments are used to characterize the electronic properties of Tb in $Pb_2Sr_2TbCu_3O_8$. The x-ray absorption results indicate that Tb is trivalent and show no evidence for strong hybridization between Tb and the CuO_2 bands. The observation of three peaks of magnetic origin in the INS experiments is also a clear indication of the trivalent state of Tb. These peaks are assigned to crystalline electric-field (CEF) transitions, and their energies and intensities are consistent with the CEF potential expected for a trivalent rare earth in the $Pb_2Sr_2RCu_3O_8$ lattice. The low-energy response in the INS spectra at low temperatures is described using the mean-field approximation. Single crystal and polycrystalline susceptibilities show deviations from calculations and differ from magnetically diluted samples. These deviations are observed for temperatures less than 120 K and we interpret this as the onset temperature of the magnetic Tb-Tb short-range correlations. This interpretation is supported by the temperature dependence of the magnetic INS intensities at low energies. The onset temperature, estimated at 120 K, is more than an order of magnitude higher than seen in any related system, as well as much higher than the two-dimensional long-range ordering temperature at $T=5.5$ K. This unusual behavior is understood in terms of the highly two-dimensional nature of the lattice combined with the strongly Ising-like magnetic properties. In addition to the Tb-Tb correlations, the susceptibility experiments on a magnetically dilute sample indicate a weak rare-earth Cu exchange interaction.

I. INTRODUCTION

Rare-earth-doped high-temperature superconductors exhibit a wide range of interesting magnetic properties. The rare-earth sublattice may show three-dimensional long-range,[1,2] three-dimensional with finite correlation length,[3] two-dimensional[4,5] (2D), and hyperfine-induced magnetic ordering.[3] In addition, some superconductors, or their parent compounds, exhibit 2D short-range correlations well above the Néel temperature.[6] One of the most interesting systems is $Pb_2Sr_2TbCu_3O_8$ with a 2D Néel temperature of $T_N=5.5$ K and short-range correlations reported up to 10 K.[6] Short-range correlations of the rare-earth spins well above T_N were also reported by means of calorimetric experiments on $Pb_2Sr_2PrCu_3O_8$.[7] The interplay between the rare-earth magnetism and superconductivity remains unclear, although the superconducting properties appear relatively uninfluenced by the presence of the local f moments.

For a better understanding of the magnetic properties of these materials, information on the magnetic ground-state wave function and on the rare-earth exchange interactions are required. The rare-earth ground-state wave function can be extracted from the measurements of crystalline electric-field (CEF) excitations by inelastic neutron scattering (INS). Whereas this information is already available for most of the rare earths in the $RBa_2Cu_3O_X$ series,[8,9] it is missing for $R=$Tb, because this compound does not form. It has previously been suggested that the relative stability of tetravalent or intermediate-valent Tb could explain why $TbBa_2Cu_3O_x$ does not form.[10] However, a recent x-ray absorption and magnetization study has determined a 3+ valence for Tb in $Tb_{0.1}Y_{0.9}Ba_2Cu_3O_x$, with no indication of any significant hybridization between Tb and the CuO_2 bands.[11] In that work it was concluded that the stability of $BaTbO_3$ during the solid-state reaction prevents the formation of $TbBa_2Cu_3O_x$.

Some qualitative information on the exchange interaction can be obtained from low-temperature magnetization and specific-heat measurements.[12] A more detailed insight into the coupling mechanism requires a study of the spin waves, which inherently contain information on the nature and size of the magnetic coupling between R^{3+} ions. INS provides the most direct information on spin waves; however, the only two systems studied so far are the superconducting $HoBa_2Cu_3O_7$,[13,14] and the parent compound Pr_2CuO_4.[15]

$Pb_2Sr_2RCu_3O_8$ ($R=$rare earth) are layered materials that are structurally complex, but basically similar to other copper oxide systems such as the $RBa_2Cu_3O_x$ series or the Tl- and Bi-based cuprates. In the Pb-based series, the $R=$Tb analog does form, and by replacing 50% of R by Ca the material can be made to superconduct with a T_c around 80 K. There are relatively few studies directed toward understanding the underlying electronic and magnetic properties of these series;[7,16–18] however, two INS studies on $Pb_2Sr_2HoCu_3O_8$ and $Pb_2Sr_2Er_{1-x}Ca_xCu_3O_8$ ($x=0$ and 0.5) are reported in the literature.[19,20] In these studies the CEF potentials were determined and the related magnetic properties were calculated.

In this work, we report x-ray absorption, INS, and magnetic susceptibility experiments to clarify the valence and possible hybridization of Tb. In addition, these data are used to determine the ground-state wave functions of Tb in order to help in the development of a better under-

standing of the short-range fluctuations observed well above T_N. The susceptibility experiments indicate an onset of two-dimensional short-range spin correlations around 120 K, in good agreement with the INS experiments. This temperature is more than an order of magnitude higher than observed in any related system. In addition, it is also an order of magnitude higher than the long-range 2D ordering at $T=5.5$ K found by neutron diffraction.[6]

II. EXPERIMENTS

Polycrystalline $Pb_2Sr_2Tb_{1-x}Y_xCu_3O_8$ samples were prepared by first weighing out stoichiometric amounts of PbO, Tb_4O_7, Y_2O_3, CuO, CaO, and $SrCO_3$, followed by intimate mixing in an agate ball mill, pelletizing, and sintering at 830 °C for 20 h. After furnace cooling to room temperature, we checked the samples with x-ray diffraction. Milling, pelletizing, and sintering procedures were repeated until the x-ray diffraction pattern verified the single-phase character of the samples. Neutron diffraction on the same samples confirmed their single-phase nature. The single-crystal growth is explained in detail elsewhere.[21]

Tb L_3-edge (7514 eV) x-ray absorption near-edge structure (XANES) data were collected at ambient temperature on beamline X-23A2 at the National Synchrotron Light Source. X-23A2 is equipped with a Si⟨311⟩ double-crystal monochromator to provide good energy resolution[22] ($\Delta E/E=2.90\times10^{-5}$) and effective harmonic rejection of the second-order Bragg reflection. A 1 mm premonochromator vertical slit was employed, resulting in a calculated total-energy bandwidth of 1.5 eV at 7514 eV. With this configuration, the instrumental resolution is ca. 2.8 times smaller than the natural linewidth (4.12 eV) of the Tb L_3 core hole.[23] Hence, the Tb L_3-edge XANES is expected to be only slightly broadened ($\leq 6\%$) by the instrumental-resolution function. To obtain edge resonance intensities and positions that are not compromised by sample thickness effects, the XANES was detected using the electron-yield method.[24] Powder specimens were pressed into the adhesive of aluminized Mylar tape, which was then attached to the back plane of the electron-yield detector (The EXAFS Company). Helium was used as the ionization gas for the electron-yield signal I_e and nitrogen was used to monitor I_0.

Inelastic neutron scattering experiments were carried out on the High-Resolution Medium-Energy Chopper Spectrometer (HREMCS) at the Intense Pulsed Neutron Source (IPNS) of Argonne National Laboratory. The incident neutron energy (E_i) was chosen to be either 4 or 80 meV so that the energy resolutions at 0 and at 40 meV energy transfer are 0.17 and of 2.4 meV for $E_i=4$ and 80 meV, respectively. The powder sample of $Pb_2Sr_2TbCu_3O_8$ was enclosed in a flat aluminum container and then attached to the cold finger of a closed-cycle refrigerator to achieve temperatures of 20–300 K. A conventional helium cryostat was used for the low-temperature experiments ($1.7\leq T\leq 20$ K). The raw data have been corrected for detector efficiency and background by standard procedures. Neutron absorption by the sample was negligible.

The magnetic susceptibility experiments were performed on a superconducting quantum interference device (SQUID) magnetometer over the temperature range of 10–300 K using an applied field of 500 Oe. An ~1 mg single crystal was attached directly to a quartz fiber. Measurements were made with the "long" crystallographic c axis perpendicular and parallel to the applied field. Pellets of about 100 mg were used for the measurements on polycrystalline samples. A $Pb_2Sr_2YCu_3O_8$ sample was measured and the normalized susceptibility was then subtracted from the Tb-containing data to isolate the magnetic response of Tb alone. This step was necessary for the low Tb concentrations, where the copper sublattices provide a significant contribution to the overall measured susceptibility.

III. L_3-EDGE X-RAY ABSORPTION

The measured L_3 x-ray absorption edges obtained from Tb in a variety of standards are compared with $Pb_2Sr_2TbCu_3O_8$ in Fig. 1. The Tb^{3+} spectrum of $TbCl_3\cdot6H_2O$ is composed of only one narrow peak at 7521 eV, whereas the spectrum of Tb_4O_7 is composed of two much broader peaks centered at 7522 and 7530 eV, indicative of the inhomogeneously mixed-valent nature of the sample. The Tb^{4+} edge of $SrTbO_3$ is composed of at least three unresolved transitions, the center of gravity of which is displaced to even higher energies, at 7528 eV. These observed spectral features are typical of those expected for trivalent, mixed-valent, and tetravalent Tb.[25,26] The observed peaks arise from the $2p^65d^04f^8\rightarrow2p^55d^14f^8$ and $2p^55d^04f^7$ transitions for Tb^{3+} and Tb^{4+}, respectively.[25] The peak position in $Pb_2Sr_2TbCu_3O_8$ is 7521 eV, which is typical of Tb^{3+}, and there is no evidence for a second, higher-energy transition expected for Tb^{4+}. The peak positions, together with the absence of a second absorption peak to higher energies demonstrate that the Tb is neither tetravalent

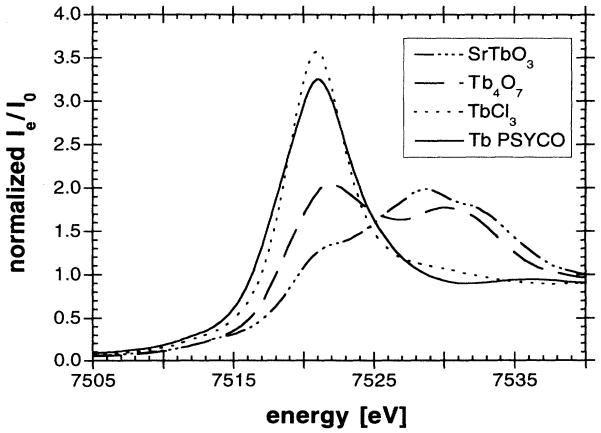

FIG. 1. Tb L_3-edge XANES of $Pb_2Sr_2TbCu_3O_8$ (PSYCO), $TbCl_3\cdot6H_2O$, Tb_4O_7, and $SrTbO_3$ obtained through electron-yield detection at ambient temperature. The first peak in Tb_4O_7 is attributed to $4f^8$ Tb(III) and the second peak to $4f^7$ Tb(IV) final states.

nor mixed valent, but instead is essentially Tb^{3+} in $Pb_2Sr_2TbCu_3O_8$. The same behavior has been observed in $Y_{0.9}Tb_{0.1}Ba_2Cu_3O_x$.[11]

A close inspection of the data presented in Fig. 1 reveals that the L_3-edge resonance of $Pb_2Sr_2TbCu_3O_8$ is slightly broader than in the spectrum for $TbCl_3 \cdot 6H_2O$. Because the L_3-absorption-edge resonance involves a transition to the bound $5d$ states just below the continuum, strong hybridization of these states may broaden the resonance.[27,28] However, there may be alternative explanations for the broadening, including changes in coordination or multiple crystallographic sites for the absorbing atom.[26] A similar broadening is found for the Tb L_3 edge in $Y_{0.9}Tb_{0.1}Ba_2Cu_3O_x$.[11] There, a careful linewidth analysis and comparison with R=Er has shown that Tb does not exhibit significant hybridization. A similar analysis of the full width at half maximum (FWHM) of the resonance in the data reported here reveals a half-width of 5.7 eV. This result is to within the error the same as that found for Tb in $Y_{0.9}Tb_{0.1}Ba_2Cu_3O_x$.[11] These data provide strong evidence that there is no significant hybridization of Tb with the CuO_2 bands.

IV. INELASTIC NEUTRON SCATTERING

A. Results

It is well known that the crystal structure of members of the $Pb_2Sr_2RCu_3O_8$ (R=rare earth) series exhibits tetragonal, orthorhombic, or even lower symmetry.[21] However, the deviations from tetragonal symmetry are small. Analysis of our neutron diffraction data on $Pb_2Sr_2TbCu_3O_8$ indicates that the crystal symmetry is orthorhombic or lower; however, the nearest-neighbor oxygens to the rare-earth ion still meet the requirements of the tetragonal-site symmetry. Therefore we assume a tetragonal-site symmetry for the CEF calculations in order to reduce the number of parameters necessary to describe the system. This assumption has previously been used for R=Ho and Er,[21] and for the crystallographically similar material $Bi_2Sr_2HoCu_3O_8$.[29] In tetragonal-site symmetry, the Tb^{3+} ground-state multiplet $^7F_6$ is split into three doublets (Γ_5) and seven singlets ($2\Gamma_1$, Γ_2, $2\Gamma_3$, and $2\Gamma_4$). A lower symmetry will further split the doublets to produce 13 singlets.

Figure 2 shows the magnetic excitation spectra of neutrons scattered from $Pb_2Sr_2TbCu_3O_8$ at T=20 K and E_i=80 meV. We observed three CEF transitions located at 30, 37, and 60 meV which are labeled by A, B, and C, respectively. The magnetic origin of these transitions is confirmed by their decreasing intensity with increasing momentum transfer Q of the neutrons (see Fig. 2). The observation of magnetic transitions in this energy range provides clear evidence for trivalent Tb, because tetravalent Tb has no orbital moment (L=0) and therefore the $J=\frac{7}{2}$ ground-multiplet is not split by the CEF to first-order. The low-energy INS spectra obtained at 1.5 K (well below T_N) and at 20 K (well above T_N) are shown in Fig. 3. There are no observable inelastic magnetic transitions at either temperature, nor is there any additional quasielastic contribution. The only difference between the two spectra is the large difference in the intensities of the elastic line. For higher temperatures we observe an additional quasielastic contribution (see Fig. 4) that increases with increasing temperature. The additional intensity is of magnetic origin as shown by its decreasing intensity with increasing Q. Transition assignments and a proposed energy-level scheme are depicted in Fig. 5.

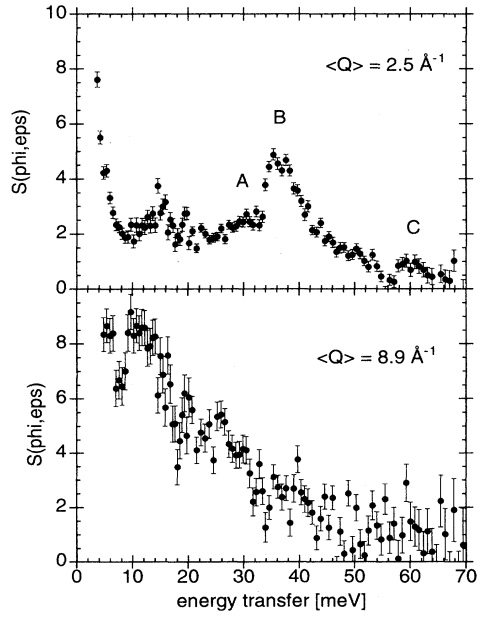

FIG. 2. Q dependence of the energy spectra of neutrons scattered from $Pb_2Sr_2TbCu_3O_8$ with E_i=80 meV and T=20 K giving rise to a $\langle Q \rangle$=2.5 Å^{-1} (top) and $\langle Q \rangle$=8.9 Å^{-1} (bottom) is determined at 37 meV energy transfer. The peak observed in the upper spectrum at about 15 meV is attributed to a phonon.

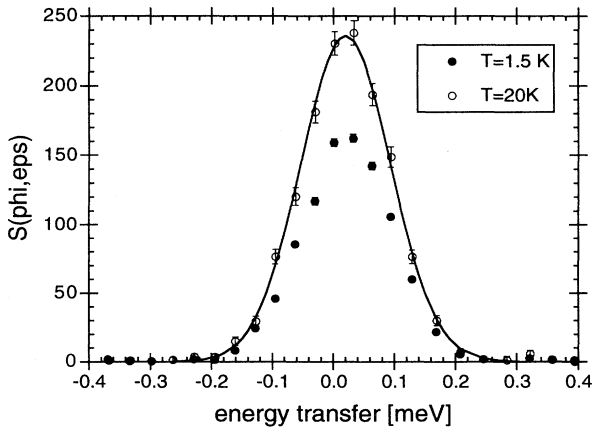

FIG. 3. Temperature dependence of the elastic line taken for $Pb_2Sr_2TbCu_3O_8$ with E_i=4 meV and $0.07 < Q < 0.44$ Å^{-1}. The line corresponds to the fitted Gaussian function.

B. Crystal-field calculations

Modeling of the CEF is carried out using standard techniques. The calculated transition energies and intensities are obtained via diagonalization of a Hamiltonian that includes the free-ion (FI) interactions, denoted by $\mathbf{H}_{el}$ and $\mathbf{H}_{SO}$, i.e.,

$$\mathbf{H}=\mathbf{H}_{el}+\mathbf{H}_{SO}+\mathbf{H}_{CEF} \tag{1a}$$

with

$$\mathbf{H}_{CEF}=\sum_{n=1}^{3}\sum_{m=0}^{n} B_{2m}^{2n}(C_{2m}^{2n}+C_{-2m}^{2n}) , \tag{1b}$$

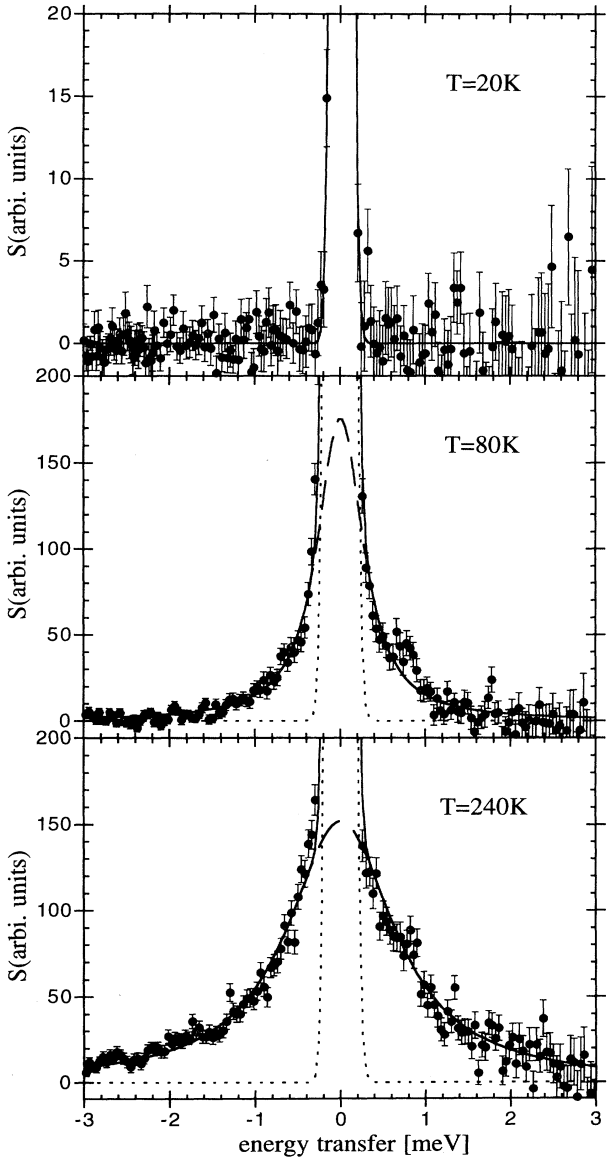

FIG. 4. Detailed-balance-corrected temperature dependence of the energy spectra from $Pb_2Sr_2TbCu_3O_8$ focused on the quasielastic contribution ($E_i=4$ meV and $0.07<Q<0.44$ Å^{-1}). The solid line corresponds to the total fit, the broken line to the quasielastic (Lorentzian), and the dotted line to the elastic (Gaussian) contribution.

using the scheme of intermediate coupling and J mixing by employing a tensor operator technique.[30] The C_{2m}^{2n} are spherical tensor operators and the B_{2m}^{2n} denote the CEF parameters. The Hamiltonian is described in more detail elsewhere.[31] The free-ion parameters were taken from those of Tb in LaF_3.[33] The tetragonal-site symmetry requires the refinement of five independent CEF parameters, namely, B_0^2, B_0^4, B_4^4, B_0^6, and B_4^6. We note here that these ratios and the CEF parameters are given in the Wyborne notation as used by Carnall *et al.*[32]

The three observed magnetic transitions lie at slightly lower energies than expected when a set of CEF parameters are extrapolated from those of $Pb_2Sr_2HoCu_3O_8$.[19] In addition to the narrow magnetic transitions, we also find strong quasielastic magnetic intensity at higher temperatures which we assign to a transition with the $\Gamma_4\rightarrow\Gamma_3$ quasidoublet. We make this assignment based on the Lorentzian line shape and the Q dependence of the quasielastic intensity. The three transition energies and their two corresponding intensity ratios yield five observables, which are not sufficient for a reliable determination of the five independent CEF parameters necessary for tetragonal-site symmetry. We therefore used a model with only three independent CEF parameters B_0^2, B_0^4, and B_0^6, and correlate the remaining two CEF parameters (B_4^4 and B_4^6) using the geometrical relations

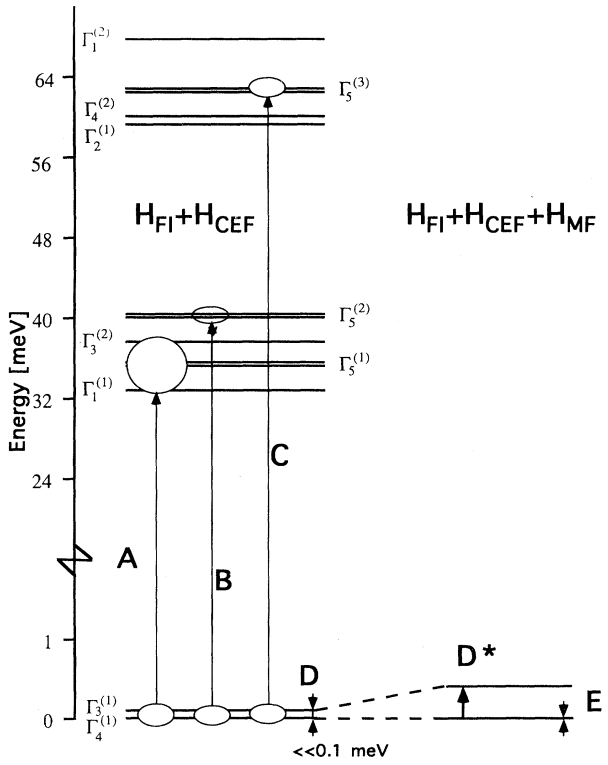

FIG. 5. Energy-level scheme of Tb^{3+} in $Pb_2Sr_2TbCu_3O_8$ calculated from the CEF parameters for the paramagnetic state (left) and the ordered state (right). The arrows denote the observed transitions and $\mathbf{H}_{FI}$, $\mathbf{H}_{CEF}$, and $\mathbf{H}_{MF}$ are explained in the text.

TABLE I. Symmetries in Koster notation (Ref. 46), observed and calculated energies, and magnetic transition strengths for the $^7F_6$ ground multiplet of Tb^{3+} in the $Pb_2Sr_2TbCu_3O_8$ lattice. [$I_{n,m}=|\langle\Gamma_4^1|\mathbf{L}+2\mathbf{S}|\Gamma_4^1\rangle|^2$ (paramagnetic state); $\Gamma_{4\mathrm{MF}}^{(1)}$ represents the former $\Gamma_4^{(1)}$ state in the molecular-field approximation (ordered state).]

$\Gamma_n^{(i)}$	E_{obs} (meV)	E_{CEF} (meV)	$I(\Gamma_4^{(1)})$	$I(\Gamma_3^{(1)})$	E_{MF} (meV)	$I(\Gamma_{4\mathrm{MF}}^{(1)})$	$I(\Gamma_{3\mathrm{MF}}^{(1)})$
$\Gamma_4^{(1)}$		0	0	74.3	0	74.3	0.0
$\Gamma_3^{(1)}$		0.007	74.3	0	0.65	0.0	74.3
$\Gamma_1^{(1)}$		31.6	0	0.0	31.9	1.3	0.0
$\Gamma_5^{(1)}$	30.2(9)	31.6	0.6	0.9	32.0	0.0	0.0
					32.0	0.0	1.0
$\Gamma_3^{(2)}$		31.9	0	0	32.3	0	0
$\Gamma_5^{(2)}$	36.7(5)	36.5	12.3	11.9	36.5	12.0	0
					37.0	0.0	12.3
$\Gamma_2^{(1)}$		51.2	0	0	51.5	0	0
$\Gamma_4^{(2)}$		56.9	0.0	0	57.2	0.0	0.0
$\Gamma_5^{(3)}$		57.1	0	0	57.5	0	0
$\Gamma_1^{(2)}$	59.9(12)	57.6	0.0	0.1	57.8	0.0	0.1
					58.0	0.1	0.0

$$B_{2m}^{2n}=B_0^{2n}\gamma_{2n}^{2m}/\gamma_{2n}^0 \ . \tag{2}$$

The coordination factors γ_{2n}^{2m}, as defined by Hutchings,[33] were calculated from the nearest-neighbor oxygen polyhedron determined by neutron diffraction:[34]

$$\gamma_4^4/\gamma_4^0=-0.5 \ ,$$

$$\gamma_6^4/\gamma_6^0=2.79 \ .$$

Because all the near neighbors are equidistant superposition modeling leads to the same ratios.[35] This modeling is expected to produce a good approximation because it has been shown repeatedly that the CEF interaction in high-T_c perovskite compounds is mainly governed by the charge distribution of the nearest-neighboring oxygen shell.[36,37] The B_0^{2n} extrapolated from $Pb_2Sr_2HoCu_3O_8$ (Ref. 19) were chosen as starting values and reproduced the characteristic features of the observed energy spectra quite well.

A least-squares refinement procedure was applied to the energies and the intensity ratios of the observed CEF transitions. It converged to the following parameters:

$$B_0^2=60\pm2 \text{ meV} \ ,$$

$$B_0^4=-235\pm5 \text{ meV} \ ,$$

$$B_0^6=61.5\pm3 \text{ meV} \ .$$

We note that these CEF parameters correspond to an axis system that has been rotated 45° around c, so that the x and y axes in this system are rotated 45° with respect to the crystallographic a and b axes. The z axis corresponds to the crystallographic c axis. The energies and the transition probabilities are listed in Table I and are compared with the observed energies. They are consistent with the energy-level scheme shown in Fig. 5. One of the remarkable features of this proposed level scheme is that the Γ_4 ground state and the Γ_3 first excited state are separated in energy by only 7 μeV. The strongest transition (B) is broader than the instrumental resolution indicating unresolved splitting of the $\Gamma_5^{(2)}$ doublet. This broadening probably originates from deviations of the true site symmetry from the tetragonal one chosen for our fitting. We do not have enough spectroscopic information to lower the symmetry of our CEF Hamiltonian to orthorhombic because this would add four more parameters. We cannot use the modeling described above to constrain the orthorhombic parameters, because the nearest-neighbor oxygen polyhedra have strictly tetragonal symmetry. However, the most important magnetic properties exhibited by the Tb sublattice are mainly influenced by the two lowest singlet states, which depend only weakly on the CEF parameters in the vicinity of the determined parameters. In addition, the CEF calculations show that the quasielastic intensity observed at elevated temperatures cannot be explained by excited CEF transitions between higher-lying states.

C. Molecular-field approximation

The CEF calculation is a good approximation, even for weakly interacting ions in the paramagnetic state. However, it has been previously reported that Tb moments are ordered antiferromagnetically at temperatures below 5.5 K. This ordering may lead to discrepancies between the observed low-energy spectra and the CEF calculations at low temperatures. In contrast to the 200 K data we do not observe the $\Gamma_4\rightarrow\Gamma_3$ transition at 1.5 K. Even when the expected energy of a CEF transition is too low in energy to observe directly, the half-width of the transition, which is broadened by relaxation, exchange, and hybridization effects, should give rise to an observable broadening of the elastic line. The full width at half maximum of the elastic line is 0.175±0.005 meV and is limited by the instrumental resolution for temperatures below 20 K. Therefore such a broadening is not observed. We can calculate the influence of the 2D magnetic long-range ordering on the CEF splitting at 1.5 K by adding a mean-field term

$$H_{MF}=\lambda\langle J\rangle^z J^z \quad (3)$$

to our Hamiltonian presented in Eq. (1a). $\langle J\rangle^z$ corresponds to the magnitude and orientation of the ordered magnetic moment, J^z is the longitudinal component of the spin operator, and λ is the mean-field (MF) parameter, which is defined as

$$\chi_0^{zz}(T_N)^{-1}=\lambda\ , \quad (4)$$

where T_N is the 2D Néel temperature of 5.5 K and χ_0^{zz} is the longitudinal component of the calculated single-ion susceptibility. Using this equation, we obtain a molecular-field parameter of 6.4 μeV. This value is slightly larger than the parameter derived for Ho^{3+} in $HoBa_2Cu_3O_7$, which was derived from the zero-field magnetization.[3] This means that the relatively high Néel temperature of 5.5 K can be understood with the same strength of the exchange interaction (λ) as in the $RBa_2Cu_3O_7$ system, supporting our conclusion that there is no significant hybridization between the Tb and the CuO_2 bands. Using this approximation, we have calculated the Tb^{3+} saturation moment and arrived at a value of $\mu_{sat}=8.40\mu_B$ at 1.5 K. This ordered moment is higher than the $(7.43\pm0.02)\mu_B$ obtained by powder neutron diffraction.[6] An overestimation of the calculated moment could be explained by the fact that the MF approximation is inadequate in the region where spin fluctuations are strong. We know that this system favors a 2D Ising type of interaction, and therefore the critical exponent for the temperature dependence of the ordered moment is expected to behave differently. The calculated energy splitting of the quasidoublet in the MF approximation is 0.64 meV at 1.5 K, and the transition strength is too small to be seen experimentally (see Table I).

D. Tb spin correlations

A striking difference between the two spectra taken at 1.5 and 20 K is the intensity of the elastic line (Fig. 3). For higher temperatures we observe an additional quasielastic contribution that increases with increasing temperature (Fig. 4) contrary to expectations. To examine this unusual temperature dependence of the elastic (Gaussian line shape) and quasielastic (Lorentzian line shape) magnetic intensities, we fitted them with a Gaussian and a Lorentzian function convolved with the Gaussian resolution function of the spectrometer. In this analysis, we include only the low-angle detectors, thereby limiting the momentum transfers to $0.07<Q<0.44$ Å^{-1}. This Q range is far below the first magnetic 2D-like Bragg reflection at $Q=1.15$ Å^{-1} ($\frac{1}{2},\frac{1}{2}$; $a\approx b\approx 3.85$ Å; following the notation used by Wu *et al.*[6]). Below 20 K, only the elastic component survives. We found that the elastic component remains resolution limited over the entire temperature range from 1.5 to 200 K. The integrated intensities of the elastic and quasielastic lines are plotted as a function of temperature in Fig. 6. The temperature dependence of the full width at half maximum is shown in Fig. 7.

At 1.5 K, in the "long-range"-ordered regime, the integrated elastic intensity corresponds to solely coherent and incoherent nuclear scattering. For higher temperatures ($T\geq 5$ K), an additional magnetic contribution is observed, and is attributed to the spreading out of the magnetic intensity in reciprocal space as a result of a decreasing correlation length of the 2D ordered moments. In the paramagnetic region, at 200 K, the observed magnetic intensity arises solely from the CEF transition between the two lowest states. It is represented by the magnetic quasielastic contribution shown in Fig. 6. Assuming no short-range correlation at $T=200$ K, the integrated Gaussian intensity corresponds to the nuclear incoherent scattering alone. 100 K represents an intermediate case, where the extra intensity of the resolution-limited elastic line must be of magnetic origin. This view is supported by the fact that the quasielastic intensity at 100 K is reduced from the 200 K level so that the overall sum of both intensities remains constant.

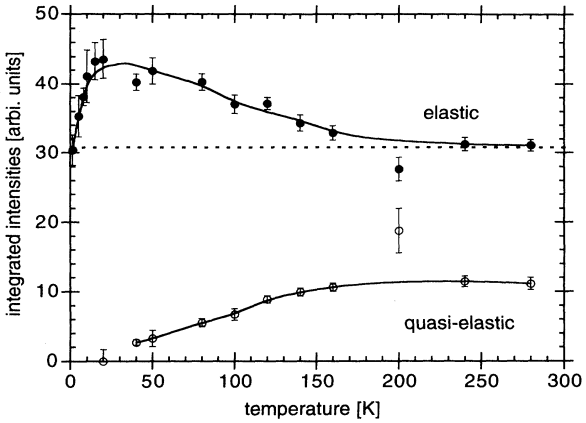

FIG. 6. Temperature dependence of the integrated elastic (open circles) and quasielastic intensity (full circles) for $0.07<Q<0.44$ Å^{-1} and $E_i=4$ meV. The solid lines are guides to the eyes. The dashed line represents the elastic nuclear incoherent scattering background.

In order to understand the relative intensity of the elastic and quasielastic components, we calculated the transi-

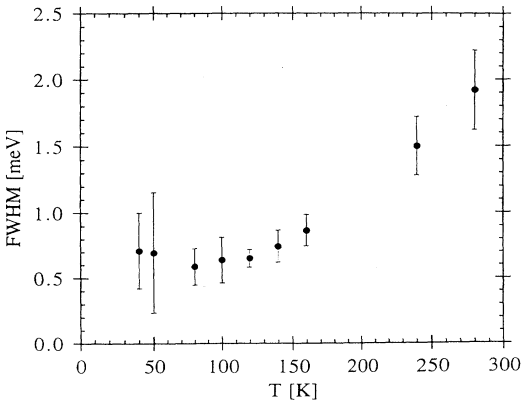

FIG. 7. Temperature dependence of the full width at half maximum of the quasielastic INS magnetic contribution determined for $Pb_2Sr_2TbCu_3O_8$.

TABLE II. Calculated transition strengths in the MF approximation for selected values of moments $g_j\langle J\rangle$. ($E=|\langle\Gamma_4^1|\mathbf{L}+2\mathbf{S}|\Gamma_4^1\rangle|^2$ and $D^*=|\langle\Gamma_3^1|\mathbf{L}+2\mathbf{S}|\Gamma_4^1\rangle|^2$ correspond to the transitions labeled in Fig. 5.)

$g_j\langle J\rangle$ (μB)	E	D^*
0	0	74.4
0.05	16.9	57.4
0.1	40.1	34.2
0.3	67.9	6.4
0.5	70.8	2.4
1	73.7	0.6

intensities within the Γ_4 ground state and between the Γ_4 and the Γ_3 states at selected values of $g_j\langle J\rangle$ within the framework of the MF approximation. The results are listed in Table II. Comparing the experiment with the calculated transition strengths, we can define three different regions. The observation for $T\leq 20$ K is well represented by the MF approximation, with a large value of $g_j\langle J\rangle$. At 100 K a short-range-ordered moment of $g_j\langle J\rangle=0.1\mu_B$ describes well the observed intensities and for $T\geq 200$ K the system is well represented by the pure paramagnetic state. We wish to note that the intensity of the Gaussian contribution reflects the size of the magnetic moment in the region of the spin correlations.

V. PARAMAGNETIC SUSCEPTIBILITY

Magnetic susceptibility experiments were carried out on $Pb_2Sr_2Tb_{1-x}Y_xCu_3O_8$ ($x=0$, 0.9, 0.95, and 0.98). The magnetic susceptibilities obtained from $Pb_2Sr_2TbCu_3O_8$ and the magnetically dilute $Pb_2Sr_2Y_{0.95}Tb_{0.05}Cu_3O_8$ are shown in Fig. 8. The data can be fitted using the Curie-Weiss law with an added temperature-independent component, $\chi=C/(T-\Theta)+\chi_{\rm TIP}$. The Curie constant ($C$) is related to the effective moment by $\mu_{\rm eff}=(8C)^{1/2}$; Θ is the Weiss constant, which is related either to changing populations in low-lying crystal-field states, or to the effect of spin-spin interactions between the magnetic ions. The $\chi_{\rm TIP}$ term represents contributions from either the Pauli or Van Vleck susceptibilities. The values obtained from fitting the experimental data are listed in Table III.

The different contributions to the measured susceptibilities can be at least partially understood by comparing the measured susceptibility with that calculated using the

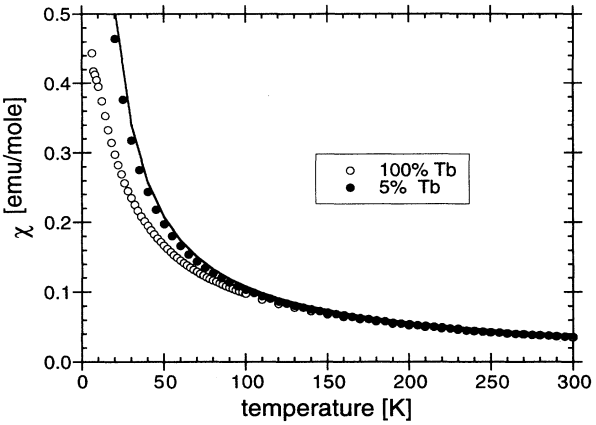

FIG. 8. Observed and calculated (line) polycrystalline susceptibilities versus temperature of $Pb_2Sr_2TbCu_3O_8$ (open circles) and $Pb_2Sr_2Y_{0.95}Tb_{0.05}Cu_3O_8$ (full circles). Susceptibility is normalized per mole Tb.

results from our INS experiments. We have used our eigenfunctions and energies determined from the CEF analysis to calculate the paramagnetic susceptibility using

$$\chi_0^{\alpha\alpha}=\frac{\mu_B^2}{k_BT}\sum_{\substack{m,n\\E_m=E_n}}|\langle n|\mathbf{L}^\alpha+2\mathbf{S}^\alpha|m\rangle|^2\rho_n$$

$$+2\mu_B^2\sum_{\substack{m,n\\E_m\neq E_n}}\frac{|\langle n|\mathbf{L}^\alpha+2\mathbf{S}^\alpha|m\rangle|^2}{E_m-E_n}\rho_n\ ,$$

where $\alpha=x,y$ corresponds to the crystal-field axis in tetragonal symmetry, as discussed earlier. $|\langle n|\mathbf{L}^\alpha+2\mathbf{S}^\alpha|m\rangle|^2$ corresponds to the transition probabilities, E_n to the energies of the states, and ρ_n is the population factor at a defined temperature. Because of the large energy separation between the quasidoublet and the higher-lying states (> 30 meV) the quasidoublet transition strength dominates the susceptibility at moderate temperatures. The results of this calculation, corrected for sam-

TABLE III. Fitted effective magnetic moments ($\mu_{\rm eff}$), Weiss constants Θ, temperature-independent susceptibility $\chi_{\rm TIP}$, and percentage of nearest-neighbor character (single ion or dimers) for the different Tb concentrations in $Pb_2Sr_2Tb_{1-x}Y_xCu_3O_8$ and the pure calculation.

	Θ (K)	($\mu_{\rm eff}$) (μ_B)	$\chi_{\rm TIP}$ (emu/mole)	Single ion (%)	Dimer (%)
$x=0$	-21 ± 1	9.7 ± 0.3	0.0006	0	
$x=0.9$	-1.9 ± 0.3	10.1 ± 0.3	0.006	65.6	29.2
$x=0.95$	-1.0 ± 0.2	9.7 ± 0.3	0.007	81.4	17
$x=0.98$	-0.9 ± 0.1	9.8 ± 0.4	0.003	92.2	7.5
CEF calc.	0.1 ± 0.1	9.0 ± 0.1	0.005	100	0
Free ion		9.72			

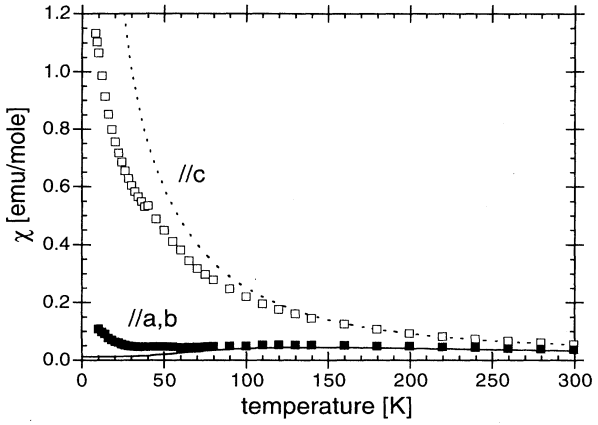

FIG. 9. Observed and calculated (line) single-crystal susceptibilities of $Pb_2Sr_2TbCu_3O_8$ (open squares $\|c$, full squares $\|a,b$).

ple diamagnetism, are compared with the experimentally determined susceptibilities in Fig. 8. In addition, the results of a fit of the calculated susceptibility, using the same modified Curie law as used for the experimental data, are included in Table III. In Fig. 9 we compare the single-crystal susceptibilities of Tb in $Pb_2Sr_2TbCu_3O_8$ with the calculation.

The observed single-crystal susceptibilities exhibit a strong anisotropy between the in-plane $\chi^{\perp}$ and out-of-plane $\chi^{\|}$ components, which is well reproduced by the calculation. The much stronger $\chi^{\|}$ component indicates the importance for the Ising type of rare-earth exchange interaction in this system. The calculations show also that this anisotropy originates from the crystalline electric field imposed by the ligands. The observed $\chi^{\|}$ deviates considerably from the calculation at temperatures below about 120 K, similarly to the powder data. The upturn in the observed $\chi^{\perp}$ around 30 K can be understood in terms of an additional transverse component in the longitudinal transition between the two lowest CEF states.

It can be seen that there is relatively good agreement between calculated susceptibility and the powder data from both Tb concentrations at temperatures higher than about 150 K. The effective moment, determined from the temperature dependence, is somewhat lower in the calculation, and may reflect a local-moment contribution to the susceptibility from the CuO sublattice. For temperatures less than 120 K, the calculations represent well the 5% Tb sample, but are very different from the pure $Pb_2Sr_2TbCu_3O_8$ sample. We interpret this discrepancy as due to the effects of Tb-Tb spin interactions that persist to very high temperatures. These interactions are strongly suppressed in the diluted system. This interpretation is consistent with the observation of an unusual temperature dependence of the INS elastic line, as described in Sec. IV.

The Θ value determined from the calculated susceptibility is clearly outside the experimental error of the Θ's derived from the measured susceptibilities. The large difference between the observed Θ's from the pure and diluted samples is understood as reflecting the decrease in spin correlations and not a crystal-field effect because the calculated susceptibility has a negligible Θ value. Because of the strong dilution (see Table III for calculated percentages of single ions and dimers) we do not expect any long-range interaction between the Tb spins. We suggest that the Θ observed for the dilute samples reflects the strength of the interaction between the rare-earth and the Cu spins. This is expected to be a weak effect because we do not see evidence in the Tb L_3-edge data for strong Tb hybridization. The distinctly higher Θ value of the 10% Tb compound may indicate that for this Tb concentration there are still some Tb-Tb correlations present at low temperatures. The Θ derived from the $Tb_{0.1}Y_{0.9}Ba_2Cu_3O_7$ ($\Theta=-1.8$ K) is similar in size.[11] A recent INS experiment reveals a similar behavior in the INS spectra.[38] Indication of a rare-earth–Cu spin interaction was also found in Refs. 39 and 40.

VI. DISCUSSION

Our INS and magnetic susceptibility data show that there are very strong Tb-Tb short-range correlations in $Pb_2Sr_2TbCu_3O_8$ that persist to temperatures up to at least 120 K, much higher than the reported Néel temperature of 5.5 K. This system exhibits these correlations up to such high temperatures for several reasons. The very strong magnetic anisotropy exhibited by the Tb^{3+} ions couples with the two-dimensional crystalline structure. The 2D ordering at low temperatures can be understood by a relatively strong 2D exchange interaction coupled with a weak dipole interaction parallel to the c axis that partly overcomes the thermal motion of the spins below 5.5 K. The 3D magnetic structure with finite correlation length can be seen in the powder neutron diffraction pattern obtained at $T=1.5$ K, where the broad, asymmetric magnetic reflections $(\frac{1}{2},\frac{1}{2},2)$ and $(\frac{1}{2},\frac{1}{2},3)$ are observed.[6] A weak dipole interaction ferromagnetically couples the Tb moments, which lie parallel to c, along this direction. The two lowest CEF states have the correct symmetry to be correlated strongly by a relatively small, Ising-type interaction. This, together with $J_{\perp} \gg J_{\|}$, gives rise to the unusual magnetic properties exhibited by Tb in this system. Additional experimental information about the exchange interactions in these materials would further the understanding of the unusually high onset temperature for the spin correlations. $HoBa_2Cu_3O_7$ is the only related system in which the exchange parameters have been determined.[13,14] It was found that the Ising-like exchange, which is defined as

$$\mathbf{H}=-\frac{1}{2}\sum_{i>j} J_{i,j}^{zz}\mathbf{J}_i^z\mathbf{J}_j^z \ , \tag{5}$$

is relatively strong with $J_a^{zz}=-6.9$ μeV,[14] even though this system does not favor an Ising type of interaction because of the symmetry of the two lowest CEF states. This result further supports our argument that the Ising type of interaction is important in the system under investigation here.

The broadening of the quasielastic contribution, as shown in Fig. 7, reflects the effect of temperature on the

CEF transition within the quasidoublet ground state and contains information about the relaxation mechanism. The half-width of the CEF transitions is directly proportional to the imaginary part of the spin susceptibility determined by the copper spins.[41] Osborn and Goremychkin[42] found an opening of an energy gap above the superconducting transition temperature by measuring the temperature dependence of the CEF half-width in $TmBa_2Cu_3O_7$. Because $Pb_2Sr_2TbCu_3O_8$ is an insulator (i.e., no carriers present) the relaxation mechanism is presumably dominated by the interaction with the copper spins. The temperature dependence of the full width at half maximum shown in Fig. 7 is constant at low temperatures, and begins to increase above about 120 K. (We note that the distinctly smaller intensities at low temperatures give rise to bigger error bars for the experimentally observed half-widths.) As it was shown by Becker, Fulde, and Keller[41] the temperature dependence of the quasielastic contribution should be proportional to T (for a Fermi liquid). Our experimental results on the insulating $Pb_2Sr_2TbCu_3O_8$ do not show a linear behavior and further work on the interaction between the rare-earth and the ordered copper spins has to be performed for an accurate description of the temperature dependence in this system.

Despite the evidence presented here of strong Tb-Tb correlations, the superconducting properties of Ca-doped $Pb_2Sr_2Tb_{0.5}Ca_{0.5}CuO_8$,[43,44] or vacancy-doped $Pb_2Sr_2Tb_{1-x}CuO_8$,[45] appear indistinguishable from the other superconducting members of these series. This is a further indication that the energetics of the correlations are weak. The Tb-Tb correlations are observable to such high temperatures in this system because it favorably combines the very two-dimensional structure with an Ising-like spin system.

VII. CONCLUSIONS

We have analyzed L_3-edge x-ray absorption near-edge structure, inelastic neutron scattering, and susceptibility data obtained from the high-T_c parent compound $Pb_2Sr_2TbCu_3O_8$. All experiments are well understood in terms of Tb^{3+} with no significant hybridization, similarly to the results of Tb doped in $YBa_2Cu_3O_x$.[11] The CEF parameters have been determined and we were able to describe the low-energy response in the INS spectra within the mean-field approximation. The INS and the susceptibility experiments both show evidence of Tb-Tb short-range correlations at temperatures above 100 K, which is more than an order of magnitude higher than the 2D magnetic ordering previously observed at 5.5 K. The susceptibility experiments on a magnetically dilute sample indicate a weak rare-earth–Cu exchange interaction. The very unusual magnetic behavior is attributed to the combination of a two-dimensional lattice and the very strongly anisotropic, Ising type of exchange interaction in this particular system. Despite these apparent Tb-Tb and Tb-CuO exchange interactions, the superconducting behaviors observed for the doped Tb/Ca samples and the Tb-deficient samples $Pb_2Sr_2Tb_{1-x}Cu_3O_8$ are not anomalous when compared to other R in the same series.

ACKNOWLEDGMENTS

The authors wish to thank J. Simon Xue for loan of the single crystal, U. Welp (ANL) for help with the SQUID measurements, J. Woicik (NIST) for assistance on X-23A2 at NSLS, L. R. Morss (ANL) for providing the Tb^{4+} standard, and Farrel Lytle (The EXAFS Co.) for helpful discussion. This work has benefited from the use of the Intense Pulse Neutron Source at Argonne National Laboratory, and financial support by DOE–Basic Energy Sciences–Chemical Sciences, all under Contract No. W-31-109-ENG-38. The Swiss National Science Foundation is gratefully acknowledged. The research was carried out, in part, at the National Synchrotron Light Source, which is supported by the U.S. Department of Energy, Division of Material Sciences and Division of Chemical Sciences.

[1]J. W. Lynn, in *High Temperature Superconductivity,* edited by J. W. Lynn (Springer, Berlin, 1990), p. 268.

[2]B. Roessli, P. Allenspach, P. Fischer, J. Mesot, U. Staub, H. Maletta, P. Brüesch, C. Ritter, and A. W. Hewat, Physica C **180&181**, 396 (1992).

[3]B. Roessli, P. Fischer, U. Staub, M. Zolliker, and A. Furrer, Eur. Phys. Lett. **23**, 511 (1993).

[4]J. W. Lynn, J. Alloys Compounds **181**, 419 (1992).

[5]B. Roessli, P. Fischer, M. Zolliker, P. Allenspach, J. Mesot, U. Staub, A. Furrer, E. Kaldis, B. Bucher, J. Karpinski, E. Jilek, and H. Mutka, Z. Phys. B **91**, 149 (1993).

[6]S. Y. Wu, W. T. Hsieh, W.-H. Li, K. C. Lee, J. W. Lynn, and H. D. Yang, J. Appl. Phys. **75**, 7124 (1994).

[7]J. H. Shieh, H. C. Ku, and J. C. Ho, Phys. Rev. B **50**, 3288 (1994).

[8]U. Staub, J. Mesot, M. Guillaume, P. Allenspach, A. Furrer, H. Mutka, Z. Bowden, and A. D. Taylor, Phys. Rev. B **50**, 4068 (1994).

[9]L. Soderholm, C.-K. Loong, and S. Kern, Phys. Rev. B **45**, 10062 (1992).

[10]G. Cao, J. W. O'Reilly, J. E. Crow, R. J. Kennedy, and D. H. Nichols, J. Appl. Phys. **75**, 6328 (1994).

[11]U. Staub, M. R. Antonio, L. Soderholm, M. Guillaume, W. Henggeler, and A. Furrer, Phys. Rev. B **50**, 7085 (1994).

[12]K. N. Yang, J. M. Ferraira, B. W. Lee, B. M. Maple, W. H. Li, J. W. Lynn, and R. W. Erwin, Phys. Rev. B **40**, 10963 (1989).

[13]U. Staub, F. Fauth, M. Guillaume, J. Mesot, A. Furrer, P. Dosanjh, and H. Zhou, Eur. Phys. Lett. **21**, 845 (1993).

[14]U. Staub, F. Fauth, M. Guillaume, J. Mesot, A. Furrer, P. Dosanjh, H. Zhou, and P. Vorderwisch, J. Appl. Phys. **75**, 6334 (1994).

[15]I. W. Sumarlin, J. W. Lynn, T. Chattopadhyay, S. N. Barilo, and D. I. Zhigunov, Physica C **219**, 195 (1994).
[16]C. R. Shih, T. H. Meen, Y. C. Chen, and H. D. Yang, Phys. Rev. B **50**, 9619 (1994).
[17]K. W. Liaw, T. H. Meen, Y. C. Chen, W. H. Lee, and H. D. Yang, Jpn. J. Appl. Phys. Lett. **32**, L1225 (1993).
[18]R. Wegerer, C. Thomsen, T. Ruf, E. Schonherr, M. Cardona, M. Reedyk, J. S. Xue, J. E. Greedan, and A. Furrer, Phys. Rev. B **48**, 6413 (1993).
[19]L. Soderholm, C.-K. Loong, J. S. Xue, J. P. Hammonds, J. E. Greedan, and M. Maric, J. Appl. Phys. **73**, 6314 (1993).
[20]L. Soderholm, C.-K. Loong, U. Staub, S. Skanthaklumar, J. S. Xue, J. P. Hammonds, J. E. Greedan, and M. Maric, Physica C **246**, 11 (1995).
[21]J. S. Xue, M. Reedyk, A. Dabbowska, J. E. Greedan, and C. H. Chen, J. Cryst. Growth **113**, 371 (1991).
[22]T. Matsushita and H. Hashizume, in *Handbook on Synchrotron Radiation,* edited by E. E. Koch (North-Holland, Amsterdam, 1983), Vol. 1A, p. 261.
[23]M. O. Krause and J. H. Oliver, J. Phys. Chem. Ref. Data **8**, 329 (1979).
[24]F. W. Lytle, in *Applications of Synchrotron Radiation,* edited by H. Winick, D. Xian, M. H. Ye, and T. Huang (Gordon and Breach, New York, 1989), Vol. 4, p. 135.
[25]M. Gasgnier, G. Schiffmacher, L. Albert, P. E. Caro, H. Dexpert, J. M. Esteva, C. Blancard, and R. C. Karnatak, J. Less-Common Met. **156**, 59 (1989).
[26]J. Röhler, in *Handbook on the Physics and Chemistry of Rare Earths,* edited by K. A. Gschneider, Jr., L. Eyring, and S. Hüfner (North-Holland, Amsterdam, 1987), Vol. 10, p. 453.
[27]O. Strebel, P. Sladeczek, M. Asensio, C. Laubschat, A. Kolodzieczyk, R. Miranda, and G. Kaindl, Physica C **162-164**, 1331 (1989).
[28]F. W. Lytle, Ber. Bunsenges. Phys. Chem. **91**, 1251 (1987).
[29]U. Staub, P. Allenspach, J. Mesot, A. Furrer, R. Müller, T. Schweizer, L. J. Gauckler, H. Blank, and H. Mutka, Z. Phys. B **85**, 35 (1991).
[30]B. R. Judd, *Operator Techniques in Atomic Spectroscopy* (McGraw-Hill, New York, 1963).
[31]J. Mesot, P. Allenspach, U. Staub, A. Furrer, H. Mutka, R. Osborn, and A. Taylor, Phys. Rev. B **47**, 6027 (1993).
[32]W. T. Carnall, G. L. Goodman, K. Rajnak, and R. S. Rana, J. Chem. Phys. **90**, 3443 (1989).
[33]M. T. Hutchings, in *Solid State Physics: Advances in Research and Applications,* edited by F. Seitz and D. Turnbull (Academic, New York, 1964), Vol. 16, p. 227.
[34]S. Skanthakumar, L. Soderholm, and U. Staub (unpublished).
[35]D. J. Newman, Adv. Phys. **20**, 197 (1971).
[36]A. Furrer, P. Brüesch, and P. Unternährer, Phys. Rev. B **38**, 4616 (1988).
[37]V. Nekvasil, Solid State Commun. **65**, 1103 (1988).
[38]U. Staub and L. Soderholm (unpublished).
[39]M. Guillaume, U. Staub, F. Fauth, J. Mesot, A. Furrer, and C. J. Carlile, Physica C **223**, 333 (1994).
[40]I. N. Kurkin, I. K. Salikhov, L. L. Sedov, M. A. Teplov, and R. S. Zdanov, Zh. Eksp. Teor. Fiz. **103**, 1342 (1993) [Sov. Phys. JETP **76**, 657 (1993)].
[41]K. W. Becker, P. Fulde, and J. Keller, Z. Phys. B **28**, 9 (1977).
[42]R. Osborn and E. Goremychkin, Physica C **185-189**, 1179 (1991).
[43]L. F. Schneemeyer, R. J. Cava, A. C. W. P. James, P. Marsch, T. Siegrist, J. V. Waszczak, J. J. Krajewski, W. P. Peck, Jr., R. L. Opila, S. H. Glarum, J. H. Marshall, R. Hull, and J. Bonar, Chem. Mater. **1**, 548 (1989).
[44]S. Skanthakumar (unpublished).
[45]J. Simon Xue, Ph.D. dissertation, McMaster University, Hamilton, Canada, 1992.
[46]G. F. Koster, *Space Groups and Their Representations* (Academic, New York, 1957).